Entropy-driven Orientational Order Of Topologically Modified Polymers In Confinement

A Thesis

submitted to
Indian Institute of Science Education and Research Pune
in partial fulfillment of the requirements for the
BS-MS Dual Degree Programme

by

Sanjay Bhandarkar

Indian Institute of Science Education and Research Pune
Dr. Homi Bhabha Road,
Pashan, Pune 411008, INDIA.

April, 2024

Supervisor: Dr. Apratim Chatterji

Certificate

This is to certify that this dissertation entitled **'Entropy-driven Orientational Order Of Topologically Modified Polymers In Confinement'** towards the partial fulfilment of the BS-MS dual degree programme at the Indian Institute of Science Education and Research, Pune represents study/work carried out by Sanjay Bhandarkar at Indian Institute of Science Education and Research under the supervision of **Dr. Apratim Chatterji**, Associate Professor, Department of Physics , during the academic year 2023-2024.

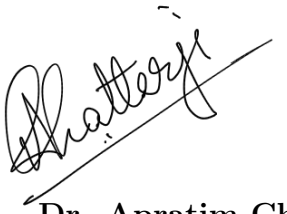

Dr. Apratim Chatterji

Committee:

Dr. Apratim Chatterji

Dr. Arijit Bhattacharyay

This Thesis is dedicated to -

My Ajja, Mr. Damodar Nayak.

Declaration

I hereby declare that the matter embodied in the report entitled Entropy-driven Orientational Order Of Topologically Modified Polymers In Confinement are the results of the work carried out by me at the Department of Physics, Indian Institute of Science Education and Research, Pune, under the supervision of Dr. Apratim Chatterji and the same has not been submitted elsewhere for any other degree. Wherever others contribute, every effort is made to indicate this clearly, with due reference to the literature and acknowledgment of collaborative research and discussions.

Sanjay Bhandarkar

Acknowledgments

Firstly, I extend my deepest gratitude to my supervisor, Dr. Apratim Chatterji, whose unwavering support, guidance, and expertise have been instrumental in bringing this thesis to fruition. Even amidst the busiest of days, he remained approachable and fostered an environment that welcomed new ideas. Our discussions have greatly helped me develop new insights and have shaped my academic growth. I remain grateful for all the help he has extended to me over the years. I would also like to thank my thesis expert, Dr. Arijit Bhattacharyay, who provided necessary insights during the project. Apart from them, I am thankful to the institute for providing all the necessary resources and facilities to complete this thesis. In particular, I acknowledge the high-performance PARAM-BRAHMA supercomputer.

I am fortunate to work alongside a remarkable group of labmates whose camaraderie has made this journey enjoyable. I sincerely thank Debarshi, Shreerang, Om, Vaibhav, Adrian, et.al for all their discussions which deepened my understanding of the subject. I am immensely grateful for my friends, who have been my pillars of support throughout this journey. I cherish the memories we have created together and am thankful for their unwavering support. Some of my closest companions in IISER include Abhijith, Abhinav, Atharva, Arjun, Gautham, Prathith, Ronedy, Shankar, Shreyas, Shridhar, Soham, Subbu, Vaishak, Varna. Lastly, I am profoundly grateful to my parents, without whom none of this would be possible. Their constant love, support, and motivation have allowed me to become who I am today.

Abstract

In the last few decades, there has been a sustained interest in understanding how systems at the nano-scale organize spontaneously or self-assemble to form higher- order structures. This project is an endeavor to study organizational properties in inherently disordered systems such as polymers. The key idea we propose is to control effective interactions by modulating polymer architecture (topology). We perform simulations of ring polymers that are confined in a cylindrical geometry. By introducing changes in the topology of each constituent polymer, we introduce subloops within the ring polymer. This modification of topology, combined with the confinement in the cylindrical geometry, induces entropic interactions between segments of neighboring polymers. These interactions drive the system of polymers to self-assemble into structures that maximize conformational entropy. We define certain vectors corresponding to each polymer and observe the orientational arrangement of these vectors. Finally, I also explore how one can analyze contact maps to gain a deeper understanding of polymeric systems. The principles of polymer physics presented in this thesis can be applied to study various properties of bacterial chromosomes.

Contents

Chapter 1

Introduction

1.1 What is Soft Matter?

Soft matter, as the name suggests, refers to a class of 'soft' materials. A key characteristic differentiating them from other materials is their ability to be easily deformed or structurally altered in response to external stimuli. Unlike metals or other crystalline solids, soft materials are often amorphous in nature and are held together by weak intermolecular forces. The interaction energies in such systems are comparable to room-temperature thermal energies. Thus, thermal fluctuations play an important role in the dynamics and organization of these systems. Soft matter systems typically have constituent particles whose size ranges from a few nanometers to microns. At these length scales, quantum effects can be largely ignored. We often use the framework of classical equilibrium and non- equilibrium statistical mechanics while studying soft matter systems.

Soft matter materials include liquid crystals, polymer solutions, gels and melts, surfactants, etc. They are found in everyday objects ranging from food such as milk and yogurt to toothpaste, soaps, and paint. However, soft matter also involves biological systems, including membranes, cells, tissues, chromosomes, etc. A major factor in the increasing significance of soft matter comes from the ability to understand and develop theoretical models of such biological systems through physical principles. Soft matter has also garnered global attention for its high potential for practical applications.

A defining characteristic of soft matter systems is self-assembly. A large number of microscopic constituents self-assemble to form mesoscopic structures. The interactions between these mesoscopic structures define the physical properties of the macroscopic material these form. Self-assembly also plays a crucial role in biology, as it is fundamental to creating numerous macromolecules necessary for cellular function. These self-assembled structures have found various applications in nanotechnology, including the fabrication of nano-devices and other functional nanomaterials. Therefore, it is imperative that we develop a deep understanding of the principles by which these structures self-assemble.

At equilibrium, the structures of these systems can be determined by the minimization of the Free Energy function. Under conditions of constant temperature and volume, the equilibrium state is decided by the global minimum of the Helmholtz free energy, which is given by

$$F = U - TS \tag{1.1}$$

Here, 'U' denotes the internal energies, 'T' denotes the temperature, and 'S' represents the system's entropy. Due to the low bond energies in soft matter systems, the enthalpic term 'U' is comparable to the entropic term 'TS.' As a result, the equilibrium structure is determined by the contention between the enthalpic and entropic terms.

1.2 Historical Overview

The first observation in soft matter was made by botanist Robert Brown in 1827 when he observed the random, irregular motion of pollen granules suspended in water through the microscope. This motion is now known as Brownian motion. Albert Einstein and Polish physicist Marian Smoluchowski developed the first understanding of Brownian motion, whereby they independently proposed that a particle suspended in a fluid must have similar thermal energy as the fluid (order of k_BT). They concluded the irregular motion of pollen grains resulted from the collision with water molecules. Today, this theory is being applied to understand a wide range of dynamical systems, from the motion of stars in galaxies to

fluctuations in financial markets.

Throughout the 20^{th} century, our knowledge of atoms, molecules, and statistical mechanics grew. In 1920, Hermann Staudinger was the first person to hypothesize that polymers are formed by linking small molecules through covalent bonds. In 1960, Drahoslav Lim and Otto Wichterle pioneered using hydrogels for biomedicine. However, the field of soft matter gained prominence following the awarding of the Nobel Prize in Physics in 1991 to French scientist Pierre-Gilles de Gennes, also known as 'one of the founding fathers of soft matter.' He was recognized for demonstrating that techniques initially devised for investigating ordered phenomena in basic systems could be extended to more intricate forms of matter, notably liquid crystals, and polymers. Soon, researchers began focusing on other soft materials, including foams, gels, colloids, etc. Since the 2000s, a large number of researchers have begun using the principles of soft matter to understand complex phenomena in biology. This led to the formation of an exciting branch of soft matter called the *Physics of Life.*

1.3 Polymers

Polymers are large macromolecules that consist of repeating subunits called monomers. Polymers in liquids continuously undergo changes in their conformation due to thermal fluctuations. Physicists often develop coarse-grained bead-spring models to study polymeric systems. Each bead often represents many chemical units of the polymer. Polymer physics looks to study their equilibrium and dynamical properties using principles from statistical mechanics.

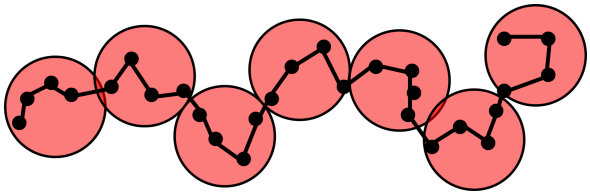

Figure 1.1: The figure represents the schematic of a coarse-grained polymer model. Each monomer(shown in red) represents four chemical units.

The statistical approach is based on a correlation between polymers and random walks. The simplest polymer model is the ideal polymer, where the constituent monomers are non-

interacting. The ideal polymer can be mapped to a simple random walk of N steps, where N is the number of monomers in the polymer. Real polymer chains have interactions between the monomers, leading to a reduction in the possible conformations of the chain. These polymers can be mapped to a self-avoiding random walk.

1.3.1 Estimating the size of polymers

As a polymer chain suspended in a fluid diffuses over time, it can take up different conformations and sizes. The equilibrium size of a polymer can be estimated by measuring the mean squared end-to-end distance $\langle R_{ee}^2 \rangle$. Where R_{ee} is defined as -

$$\vec{R}_{ee} = \sum_{i=1}^{N-1} \vec{u_i} \tag{1.2}$$

where $\vec{u_i} = \vec{r_{i+1}}$ - $\vec{r_i}$ represents the bond vector. As a polymer continuously changes configurations, we see that $\langle R_{ee} \rangle = 0$. This can be calculated by averaging over time or performing an ensemble average. Therefore, we use the mean-squared end-to-end distance $\langle {R_{ee}}^2 \rangle$ to estimate the size. Through analogy from the random walk, we see that for an ideal polymer chain,

$$\langle R_{ee}^2 \rangle = Na^2 \tag{1.3}$$

where N denotes the number of monomers in the polymer, and a denotes the equilibrium bond length[1, 2, 3]. On the contrary, for real polymer chains, the root-mean-squared end-to-end vector scales as $N^{0.58}$ in experiments. Note that when going from ideal polymers to real polymers, the exponent changes from 0.5 to 0.58, indicating that the excluded volume interactions bring additional constraints that increase the size of the polymer. Using Flory theory, one can arrive at an exponent of 0.6[4]. However, one can use more involved analytical approaches using renormalization group calculations to yield an exponent of 0.58[5].

While R_{ee} is useful for estimating the sizes of linear polymers, we cannot use this in the case of ring polymers, which do not have ends. Therefore, we use the radius of gyration R_g to characterize the size of ring, star, and branched polymers. The quantity R_g^2 is given by -

$$R_g{}^2 = \frac{1}{N}\sum_{i=1}^{N}(\vec{R}_i - \vec{R}_{com})^2 \tag{1.4}$$

where $\vec{R}_{com}$ denotes the position vector of the center of mass (COM) of the polymer.

For real chains, we find that -

$$[R_g]_{linear} \approx \frac{N^{0.6}}{\sqrt{6}} \tag{1.5}$$

$$[R_g]_{ring} \approx \frac{N^{0.6}}{\sqrt{12}} \tag{1.6}$$

1.3.2 Interaction between Monomer and Solvent

The chemical interactions between the monomers and the solvent greatly influence the characteristics of a polymer chain. The solvent can be classified into three sub-categories depending on how it interacts with the solvent:

Good Solvent

The solvent is classified as a 'good solvent' if the monomer solvent interaction is energetically favorable. In this case, the polymer swells due to excluded volume interactions, and R scales as $N^{0.6}$[1, 2].

Bad Solvent

The solvent is classified as a 'bad solvent' if the monomer solvent interaction is energeti-

cally unfavorable. In this case, the monomers avoid contact with the solvent, which induces an effective attraction between the monomers. This causes the polymer to collapse to form a globule. In this case, R scales as $N^{1/3}$[1, 2].

Theta Solvent

A theta solvent is one where the monomer and solvent interaction is such that it nullifies the swelling of the polymer chain. In this case, R scales as $N^{0.5}$, similar to ideal chains[1, 2].

It is also noteworthy that altering the system's temperature can modify the solvent's effectiveness. At elevated temperatures, the system's entropy prevails over its enthalpic interactions. In such instances, the polymer chain swells, and the solvent can be deemed a good solvent. Conversely, at lower temperatures, the interactions among monomers become more influential, potentially causing chain collapse, and the solvent may be considered a poor solvent. At intermediate temperatures, the chain's characteristic size may resemble an ideal chain, classifying the solvent as a theta solvent in this scenario.

1.3.3 Stiffness in Polymers

Polymer chains can also have varying levels of flexibility. In a flexible polymer chain, consecutive bond vectors can have any angle between them. However, semi-flexible chains constrain the bond angle formed between neighboring bond vectors. The degree of flexibility of a polymer is quantified by its persistence length. The persistence length estimates the length over which the orientation of bond vectors remains correlated[1, 2].

$$\langle cos\theta \rangle = exp(-j/L_p) \tag{1.7}$$

where θ is the angle between bond vectors $\vec{r}_0$ and $\vec{r}_j$, and L_p denotes the persistence length of the polymer chain. If the persistence length is $L_p \leq 1$, then the polymer is said to be flexible, while a persistence length larger than the contour length of the polymer suggests that the polymer is rod-like.

1.3.4 Dynamics of Polymers

The *Rouse* model describes the behavior of an ideal polymer chain over time[6]. In this model, each monomer is considered to be undergoing Brownian motion with additional constraints provided by the chain connectivity. A key assumption of the Rouse model is that the friction coefficient of the polymer $\zeta_N = N\zeta_0$, where ζ_0 is the friction coefficient of a single monomer. We can then use the Rouse model to calculate the relaxation timescale of an ideal polymer chain. We define the relaxation time τ_N as the time in which the center of mass of the polymer chain diffuses by the characteristic length R_g. The Rouse model predicts that:

$$\tau_N \approx N^2 \tau_0 \tag{1.8}$$

where N denotes the number of monomers of the polymer chain and τ_0 is the timescale in which a free monomer diffuses over unit distance.

As a monomer moves through the solvent, it displaces the solvent, causing momentum transfer through the solvent. Thus, monomers can interact over long distances via the solvent. This is called the hydrodynamic effect. The Rouse model does not consider hydrodynamic effects. Thus, it fails in the case of dilute polymers. The *Zimm* model incorporates hydrodynamic effects[7]. In the case of Zimm model :

$$\tau_N \approx N^{3/2} \tau_0 \tag{1.9}$$

It's worth noting that the Zimm model anticipates a weaker correlation between the length of the chain and the relaxation time of the polymer chain when compared to the Rouse model.

Polymers can also have different shapes, namely, linear, knotted, branched, ring, etc. These can have very different static and dynamic properties.

1.4 Ring Polymers

Researchers have devoted considerable attention to the properties of ring polymers. Unlike linear polymers, ring polymers have no ends. This topological constraint causes ring polymers to have different static and dynamic properties in dilute and melt conditions[8, 9, 10]. While understanding the dynamics of ring polymers is a fundamental problem in polymer physics, it is also important in the context of biological systems, as many bacterial chromosomes are circular. The fundamental question is, 'How does the DNA perform its functions efficiently while being confined inside the cell's nucleus?' The DNA must organize itself while avoiding entanglements and yet must be able to undergo replication, transcription, etc.

1.4.1 Role of Entropy in Polymer Segregation

Let us consider two polymers with N monomers each in a dilute solvent. Each polymer chain occupies a volume V, called the pervaded volume, corresponding to its natural size, i.e., R_g. As they are brought closer within a distance of R_g, they resist overlap due to decreased conformational entropy. Grosberg et al. showed that the free energy cost of this overlap was $F \approx k_B T$[11]. This was later confirmed by renormalization group calculations and numerical simulations[12, 13]. We find that the free energy cost is small, and the polymer chains in bulk easily intermix.

However, this free energy cost becomes significant in the presence of confinement. Let us consider two polymers intermixed within an infinitely long cylinder of $D \ll R_g$. In this case, the free energy cost of intermixing can be estimated from the 'Blob' model proposed by de Gennes[4]. We assume that the free energy cost of blob-blob overlap is of the order of $k_B T$[11]. From blob theory, we estimate the total number of blobs per chain to be around $D^{-1/\nu}$, where ν is the Flory exponent. The free energy of overlap now scales as -

$$F_{blob} \approx D^{-1/\nu} N k_B T \tag{1.10}$$

We see that entropic repulsion is a strong driving force in the presence of confinement. It scales linearly with N and is inversely proportional to $D^{1/\nu}$. It is also shown that the

timescale for segregation τ_{seg} is much smaller than the relaxation timescale τ in the same cylindrical confinement[14].

However, we know that bacterial DNA is circular. Previous works have argued that ring polymers under cylindrical confinement organize akin to a linear arrangement of blobs [15, 16, 17] of diameter $D/\sqrt{2}$ where D is the diameter of the confining cylinder. This means that rings have a higher propensity for segregation. Two spatially overlapped ring polymers in cylindrical confinement segregate spontaneously along the long axis to increase their conformational entropy[14]. Unlike eukaryotic organisms, bacteria like E.coli do not have specialized machinery responsible for DNA segregation. Thus, entropic repulsion was proposed as the mechanism governing the spatial segregation of newly formed daughter chromosomes [14, 18, 19, 20]. The two overlapping rings in a cylinder have fewer microstates than those in demixed states.

1.4.2 Significance of Loops

Detailed chromosome capture maps obtained from Hi-C[21] experiments have shown evidence of topologically associated domains (TADs) in various bacteria. The presence of loops at specific points on the genome may be responsible for these domains. Therefore, internal loops are crucial in the characteristic features observed in vivo.

It is also shown the segregation rates can be increased by suitably modifying the topology to create internal loops in the ring polymer[22, 23, 24]. The modified topology also showed that the loops get localized along the long axis of the cylinder due to mutual repulsion between the internal loops. Consequently, the position of the cross-link that creates the loops is also localized to specific positions along the long axis of the cylinder[22, 23].

In this thesis, I will discuss how one can modify polymer topology to form subloops. The entropic repulsion between internal loops can then organize different segments of the polymer. We define vectors joining the center of mass (COM) of different loops and observe the orientational ordering of these vectors. The entropic interactions between topologically modified segments of neighboring polymers lead to emergent interactions between the polymers.

Chapter 2

Model and Methods

We perform Langevin dynamics simulation of a flexible, bead-spring model of a polymer chain. This model considers a chain of spherical beads representing monomers, where each monomer is connected to two neighboring monomers by massless harmonic springs of stiffness κ and equilibrium length a. The harmonic spring potential is given by $V_{spring} = \kappa(r-a)^2$, where $\kappa = 100k_BT/a^2$. We consider a to be the unit of length in our simulation, and energies are measured in units of thermal energy k_BT. Furthermore, the excluded volume interactions between the monomers are modelled by the Weeks-Chandler-Andersen (WCA) potential[25].

$$V_{WCA} = 4\epsilon\left[\left(\frac{\sigma}{r}\right)^{12} - \left(\frac{\sigma}{r}\right)^{6}\right] + \epsilon_0, \quad \forall r < 2^{1/6}\sigma \tag{2.1}$$

where $\epsilon = k_BT$, $\sigma = 0.8$, and ϵ_0 is added to ensure the potential goes to zero smoothly at the cutoff. If the cutoff is $2^{1/6}\sigma$, then $\epsilon_0 = \epsilon$. $V_{WCA} = 0$ if r is greater than the cutoff.

For our studies, we consider one or more modified ring polymers confined within a cylinder. The interactions between the monomers and the walls of the cylinder are modeled using the WCA potential. We vary the length of the cylinder L and the diameter $D = 2R$ to create systems of varying density. We choose the diameter D such that $D \ll R_g$ of an unconfined ring polymer. We work polymer chains that have $N = 200$ monomers unless specified otherwise. We modify the topology of ring polymers by introducing cross-links (CLs) between

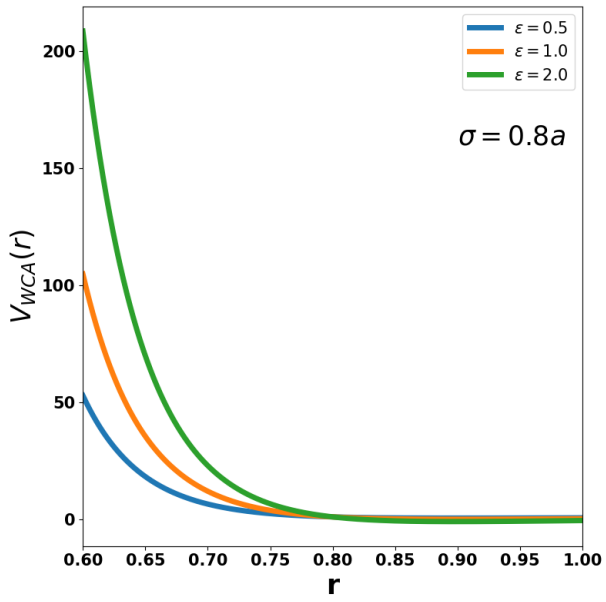

Figure 2.1: Shows a plot of the WCA potential with $\sigma = 0.8$a for different values of ϵ. The WCA potential rises sharply for values lower than σ.

specific monomers of the polymer. The cross-linking is achieved through harmonic springs of equilibrium length a and spring constant κ. This creates internal loops within the ring polymers. The details of the design of the modification are provided in the results section.

The Langevin equation[26] is given by -

$$m\frac{d^2\vec{r}}{dt^2} = -\gamma\frac{d\vec{r}}{dt} + f_{ext} + \eta(t) \tag{2.2}$$

where m denotes the particle mass, γ represents the damping coefficient, and $\eta(t)$ denotes the noise term which represents the random collisions of the fluid molecules. The noise term has a Gaussian probability distribution with a correlation function -

$$\langle \eta(t) \rangle = 0 \tag{2.3}$$

$$\langle \eta_i(t)\eta_j(t')\rangle = 2\gamma k_B T \delta_{i,j}\delta(t-t') \tag{2.4}$$

This shows that this is a Gaussian white noise proportional to thermal energy. The δ dependence tells us this noise is uncorrelated over time.

We use Langevin dynamics as implemented in LAMMPS to realize our model system[27]. We use a time step of $\delta t = 0.01\tau_0$ where $\tau_0 = \sigma\sqrt{m/\epsilon}$ is the timescale in the simulation, with the mass of the beads $m = 1$. A Langevin thermostat maintains the system at a fixed temperature of T with a damping constant of $\gamma = m/\tau = \tau_0^{-1}$.

We initialize the rings while ensuring they are segregated along the cylinder's axis and are not concatenated. To achieve this, we initialize the rings in a circle whose diameter is lesser than that of the confining cylinder. However, this leads to a significant overlap of monomers and consequently, a highly energetic configuration. Hence, we perform 10^4 Monte-Carlo Steps (MCS) to decrease the overlap and thereby reduce the energies. We then run the LD simulations for 2×10^8 iterations. We let our system equilibrate for the first 10^8 iterations and only then begin to collect data for statistical analysis. To ensure that the system has reached equilibrium in 10^8 iterations, we analyze the z-coordinate of the COM of the different segments of each polymer to confirm that each polymer flips and interchanges position multiple times over the course of the simulation. This process ensures that the polymer attains many different configurations before we collect data to calculate statistical quantities.

In each Monte-Carlo step (MCS), we perform N attempts to displace a monomer in a random direction, where N is the number of monomers in our simulation. Whether the attempt is accepted or not is determined by the metropolis algorithm. Let us assume ΔE is the change in energy of the system due to a trial displacement. If $\Delta E < 0$, the trial displacement is accepted. However, if $\Delta E > 0$, the trial displacement is accepted with a probability of $e^{\frac{-\Delta E}{k_B T}}$.

Chapter 3

Results

3.1 The Dumbbell Architecture

We begin with two ring polymers of size N = 200 each, confined in a closed cylinder of length $L = 25a$ and diameter $D = 5a$. This results in an aspect ratio of 1:5 and a volume fraction of $\phi \approx 0.218$ where

$$\phi = 2N \times \frac{\frac{4}{3}\pi(\frac{\sigma}{2})^3}{\pi R_c^2 L} \tag{3.1}$$

The diameter of the cylinder is chosen such that D is significantly smaller than the equilibrium size R_g of an unconfined ring polymer. The R_g of an unconfined ring polymer with 200 monomers can be calculated using 1.6 :

$$R_g \approx \frac{(200)^{0.6}}{\sqrt{12}} \approx 6.93a \tag{3.2}$$

We add a topological modification to the polymers by adding a cross-link (CL) between the $50th$ and $150th$ monomers of each polymer. This CL brings the diametrically opposite

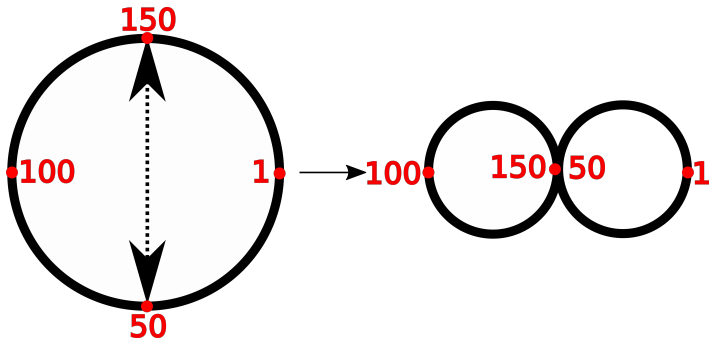

Figure 3.1: Shows a schematic of a ring polymer which we modify to create the dumbbell topology

monomers close to one another, effectively 'pinching' the ring polymer to form two smaller subloops, refer to the schematic in Fig.3.1. In the text, we refer to this topologically modified polymer as the 'dumbbell polymer.'

We calculate the COM positions of each subloop at each snapshot and plot the probability distributions of the COM positions along the z-axis in Fig.3.2. We choose the axis of the cylinder to be along z. The positional distribution of the COM shows four distinct peaks corresponding to the four subloops. This data clearly shows that the subloops are well segregated. The peak indicates that the subloops occupy different segments of the cylinder, which is a consequence of the entropic repulsion between them. We can also observe that the peaks are equidistant and are located at $\approx (L/8, 3L/8, 5L/8, 7L/8)$. We see that the subloops of the first polymer flip between $L/8, 3L/8$ positions. Similarly, the subloops of the second polymer flip between $5L/8, 7L/8$ positions. We also observe snapshots where the polymers interchange positions along the long axis. This is evidenced by a small probability of the first polymer on the right side and vice versa. We plot the COM of different subloops as a function of time in Fig.3.3. We see that the COM of different subloops are well segregated. We can also see the polymers frequently undergo flips, which interchanges the subloop's position.

An important point to note is the difference in peak heights in the COM distribution. The two peaks closer to the center are shorter when compared to the loops at the corner of the cylinder. This arises due to the fact that a subloop at the center overlaps and faces entropic repulsion from two subloops on either side. However, a subloop present towards the corner faces repulsion from a subloop on one side and a hard repulsive wall on another. As a result, the COM of the subloop at the center is spread over a wider range compared to the

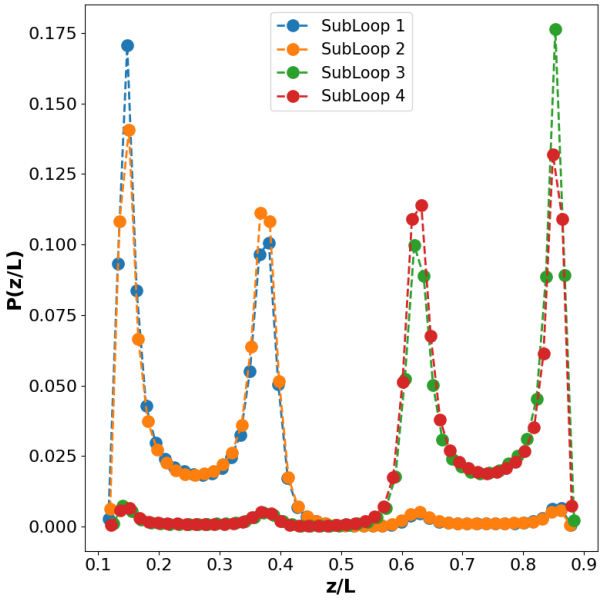

Figure 3.2: This figure shows the spatial probability distribution P(z/L) of the center of mass of each subloop with two dumbbell polymers in a cylinder of length $L = 25a$. We consider the cylindrical axis to be along the z-axis. Subloop 1 and 2 are subloops of the first polymer, while Subloop 3 and Subloop 4 are the subloops of the second polymer.

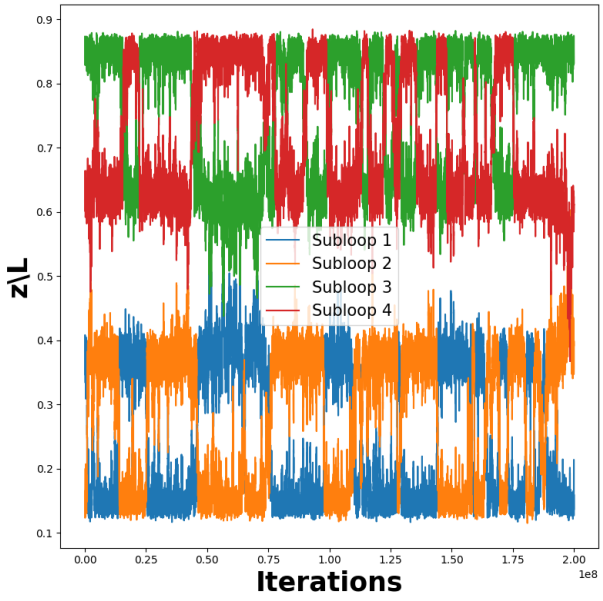

Figure 3.3: This figure shows the Z-coordinate of the COM of different subloops as a function of time. The data provided, the cylinder length is L = 25a. Subloop 1 and 2 are subloops of the first polymer, while Subloop 3 and Subloop 4 are the subloops of the second polymer

subloop at the corner. This consequently leads to a difference in the peak heights. On closer inspection of Fig.3.3, we can find evidence that justifies the asymmetry in the peak heights. We observe that the COM of a subloop that is present towards the center of the cylinder fluctuates over a wider area. At the same time, the subloops are the ends of the cylinder have a relatively smaller range of fluctuations. The COM of the subloops cannot move closer to the cylinder ends beyond a certain point without causing significant inhomogeneity in density.

To probe this further, we define a vector between the COM of subloop-1 and subloop-2 for each polymer. Moreover, we calculate the dot product of the two vectors at each snapshot of the simulation. In Fig.3.4, we show the probability distribution of $\cos(\theta)$, where θ is the angle between vectors. The probability distribution of $\cos(\theta)$ shows clear peaks at $\cos(\theta) = \pm 1$, indicating that the subloops organize so that the vectors lie parallel or antiparallel. The loops can flip, and the polymers can interchange positions along the long axis. Despite this, the polymers remain demixed. We also find that as we decrease the cylinder length from $L = 25a$ to $L = 15a$, the inequality in P($cos\theta$) also sharply decreases. It is shown that decreasing the aspect ratio of the cylinder enhances the propensity for mixing of the polymers[19]. Therefore, as we decrease the cylinder length, the localization effect of subloops is reduced, leading to a decrease in the inequality in P($cos\theta$).

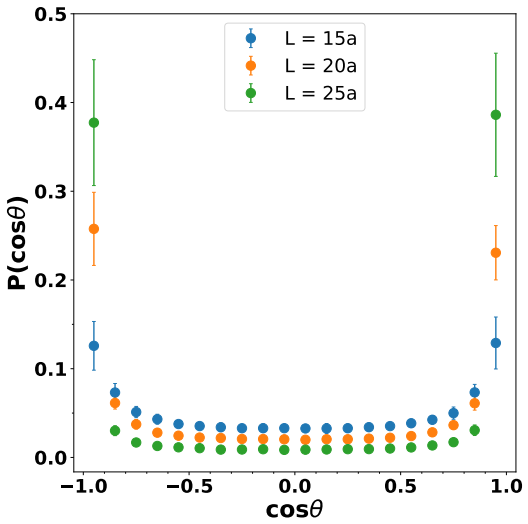

Figure 3.4: Shows the probability distribution of $cos(\theta)$ in a cylinder of varying lengths. The error bars represent the standard deviation over 40 statistically independent simulations.

Based on our understanding developed through the evidence presented so far, we provide a schematic of the configuration predominantly attained by a set of two dumbbell polymers in Fig.3.5.

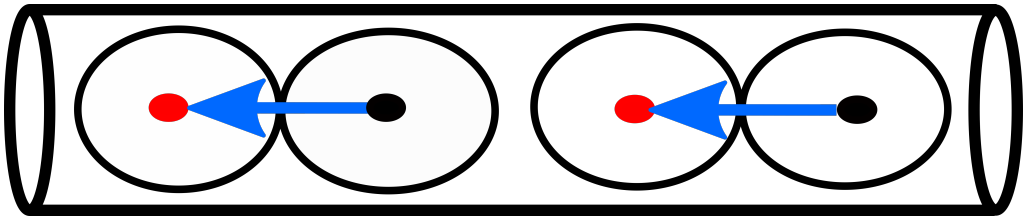

Figure 3.5: Shows a schematic of configuration predominantly attained by a set of two dumbbell polymers, where the polymer and the subloops are well segregated. The red and black dots represent the COM of the subloops. There is an equal probability of the two vectors being anti-parallel.

3.2 The Arc-1-2 Architecture

Having observed subloop localization with two 'dumbbell' polymers, we create an asymmetry in one subloop by modifying the polymer topology. We begin with two ring polymers and introduce two additional cross-links (CLs). We cross-link the monomers 1 and 50 and monomers 1 and 150 in each polymer. This leads to the formation of a bigger subloop and two smaller subloops within each polymer, refer Fig.3.6. We call this the 'Arc-1-2 Architecture'.

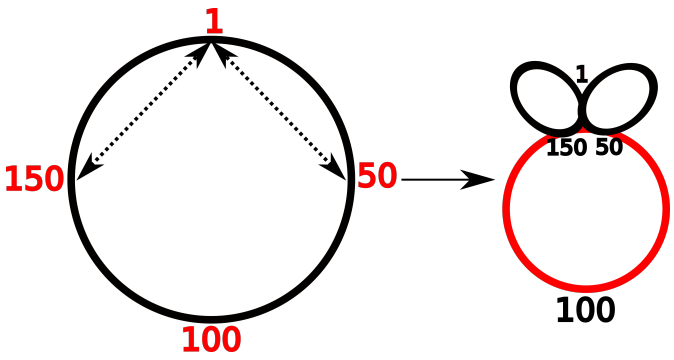

Figure 3.6: This figure shows a schematic representation of the Arc-1-2 topology.

Again, we calculate the COM positions of the big subloop and both the small subloops

considered together. We define vectors from the COM of the big subloop to the COM of the smaller subloops. We also plot the probability distribution of the COM of the big subloop and both the smaller subloops together along the z-axis; refer to Fig.3.7a. As seen previously in the investigations with a pair of dumbbell polymers, we observe (i) two polymers are well segregated along z; (ii) the COM of different loops show four distinct peaks in $p(z)$. In Fig.3.7b, we plot the probability distribution of $cos(\theta)$, which now shows a small indication of asymmetry in the probabilities of $cos(\theta) = 1$ and $cos(\theta) = -1$. This indicates a higher preference for anti-parallel configurations. This asymmetry increases as we decrease the length of cylinder $L = 25a$ to $L = 15a$.

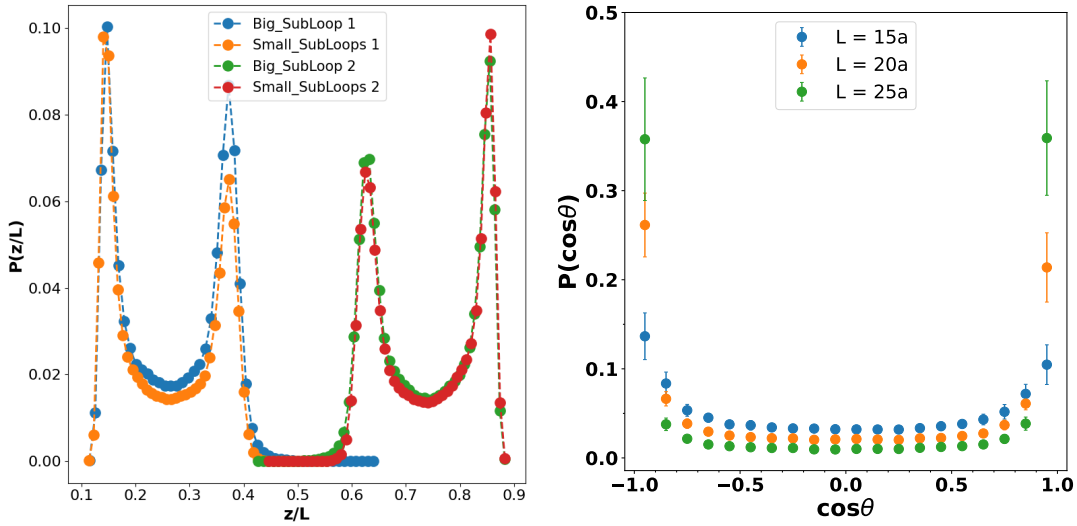

Figure 3.7: Subfigure (a) Shows probability distribution P(z/L) of the center of mass (COM) of the different loops as two Arc-1-2 polymers in a cylinder of length $L = 25a$ explore different microstates. Subfigure (b) Shows the probability distribution of $cos(\theta)$ for two Arc-1-2 polymers in cylinders of varying lengths. The error bars represent the standard deviation over 40 statistically independent simulation runs.

Now that we have introduced an asymmetry in the size of one of the subloops of the dumbbell polymer, we can classify the conformations attained by a system of two Arc-1-2 polymers into the four configurations shown in Fig.3.8. Any snapshot that involves significant mixing of polymers is placed under 'Others.' We note that in configurations $C1$ & $C2$, the vectors are parallel, while in configurations $C3$ & $C4$, the vectors are anti-parallel to one another.

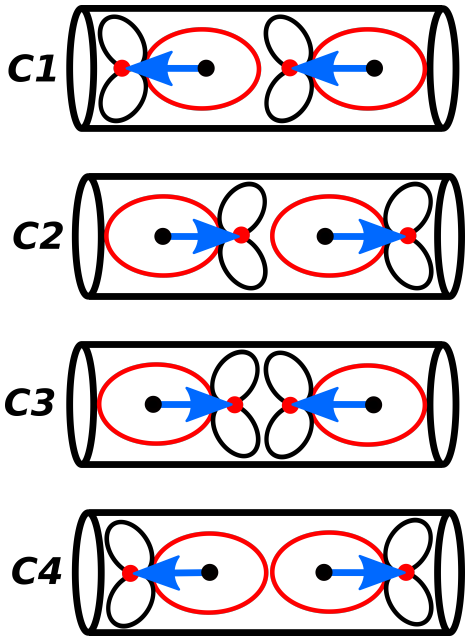

Figure 3.8: Shows the configurations that are predominantly attained by a pair of polymers having the Arc-1-2 topology. The configurations have been classified as C1, C2, C3 and C4. We note that in configurations C1 and C2, the vectors (shown in blue) are parallel, while in configurations C3 and C4, the vectors lie anti-parallel to each other.

Furthermore, as we plot the probabilities of C1, C2, C3, and C4, we find an indication of the difference in probabilities between C3 and C4. To probe this further, we choose cylinders of lengths L = 20a and L = 15a. The probabilities of the four configurations as we change the length are shown in Fig3.9a,b,c. As we go from a cylinder of length L = 25a to L = 15a, the difference in the probabilities of C3 and C4 magnifies. One must note that the probabilities C1 and C2 are identical in each case, as they involve an equivalent set of microstates. We also note that the probability of 'Others' also increases as the frequency of mixing of the polymers increases as we decrease the aspect ratio of the cylinder. We do not go to cylinders of small length as this would lead to significant mixing of the polymers. To develop a better understanding of this phenomenon, we use a cylinder of length L = 15a and plot the probability distribution of the COM positions of the different subloops along the z-axis, refer to Fig.3.11. Here, we get an indication of the tendency of bigger subloops to occupy the center. This effect persists even when considering polymers of $N = 500$ monomers, refer to SI. Fig.3.12 shows a representative snapshot of the simulation, which depicts the configuration C4, where the big loops marked by orange and brown monomers

are near the center of the cylinder, and the small loops face the axial cylindrical wall. The simulation is visualized through OVITO[28].

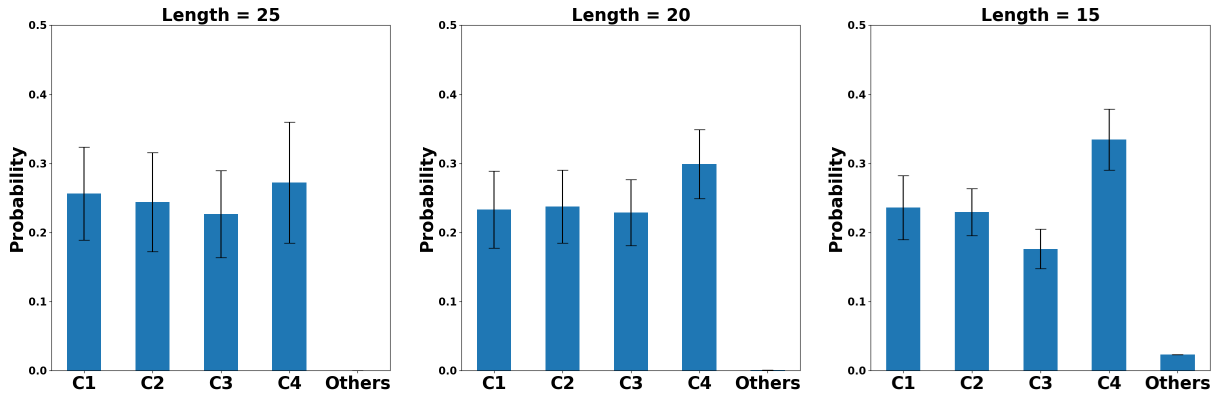

Figure 3.9: Shows the probabilities of the different configurations (C1, C2, C3 & C4) attained by two Arc-1-2 polymers in cylinders of varying lengths while keeping the diameter fixed at D = 5a. The error bars represent the standard deviation over 40 statistically independent simulations

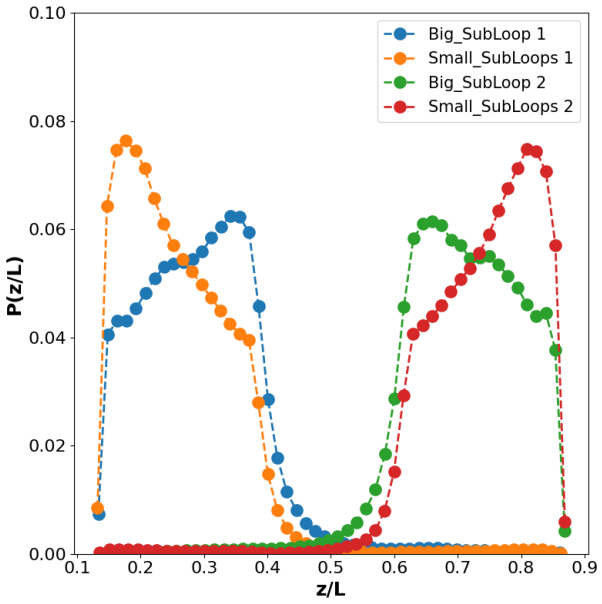

Figure 3.10: Shows the probability distribution P(z/L) of the center of mass (COM) of the different subloops as two Arc-1-2 polymers in a cylinder of length $L = 15a$ explore different microstates.

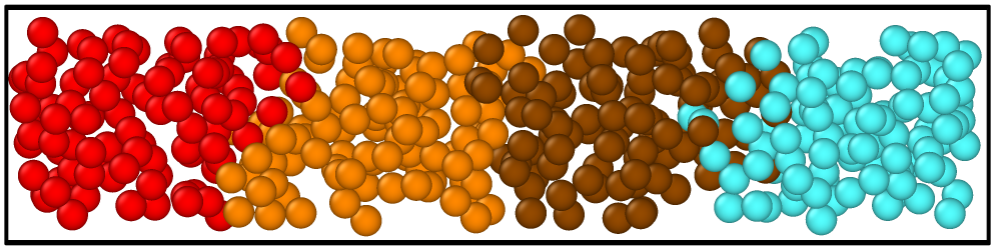

Figure 3.11: Representative simulation snapshot of two Arc-1-2 polymers reaffirming that the polymer and its subloops are well segregated along the long-axis. The monomers painted in red belong to the two small subloops of the first polymer, while the monomers in orange belong to the big subloop of the first polymer. Similarly, the monomers in brown belong to the big subloop of the second polymer, and the blue monomers belong to the small subloops of the second polymer.

3.3 Hierarchical Subloops

Here, we introduce additional cross-links (CLs) within each small subloop of the Arc-1-2 polymer to create hierarchical subloops. We study the effect of hierarchical subloops in the smaller subloops to check if this increases the tendency of the big subloop to localize towards the center of the cylinder. To investigate this, we create multiple loops of various sizes in the smaller subloops of the Arc-1-2 architecture. In Fig.3.12, we show a schematic of an Arc-1-2 polymer with an additional loop of size 20 within its small subloop. Similarly, we can also introduce multiple loops of size 5 and 10 within the small subloop and study their effect on the organization of the Arc-1-2 polymer.

We calculate the COM positions of the big subloop and small subloops at every snapshot in the simulation. Further, we plot the spatial probability distribution P(z/L) of the COM of different subloops, refer to SI. In Fig.3.13, we plot the probabilities of the different configurations (C1, C2, C3 & C4) with two modified Arc-1-2 polymers in a closed cylinder of length $L = 25a$. We note that the asymmetry between the probabilities of configuration C3 & C4 is greater than in Fig.3.9a. This indicates that we can use multiple small-size loops to enhance the propensity of the big subloops to occupy the center. However, we notice that as one begins to consider loops of length smaller than 10, the entropic repulsion provided

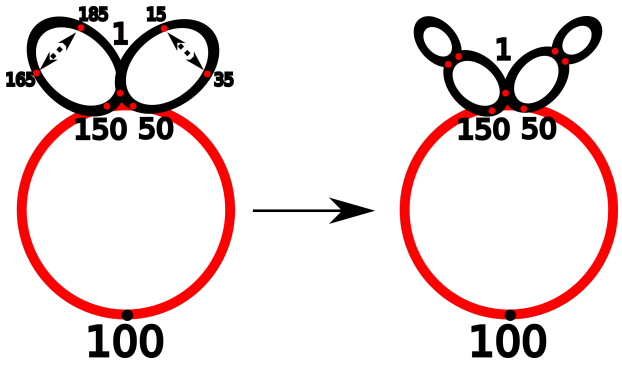

Figure 3.12: Shows a schematic of the Arc-1-2 architecture with an additional small subloop of size 20 within its small subloops.

by the loop becomes insignificant. The loops of such lengths can be considered similar to a monomer. This can be justified by analyzing Fig.3.13c. Despite introducing four loops of size 5, we do not see an increase in the difference in probabilities of C3 & C4. Hence, we choose loops with a length of 10 monomers.

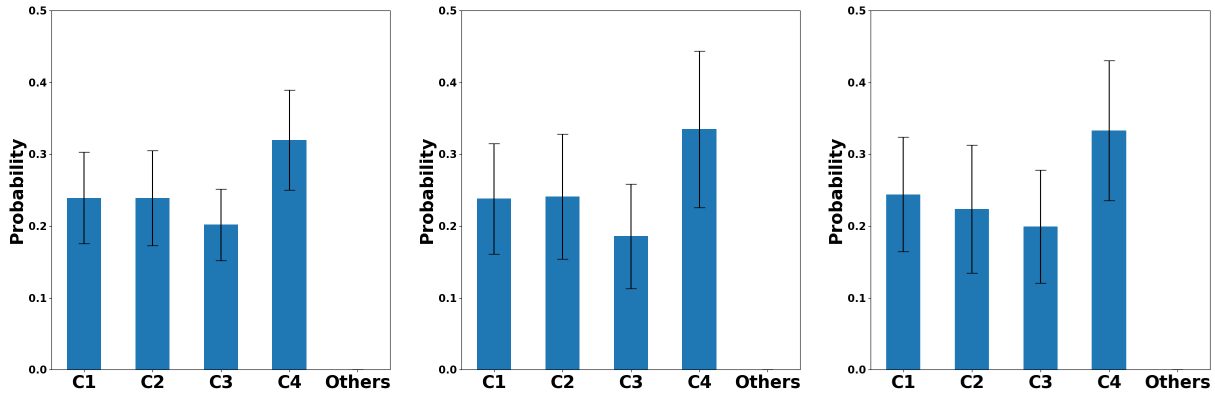

Figure 3.13: Shows the probabilities of the different configurations (C1, C2, C3 & C4) attained by two modified Arc-1-2 polymers in a closed cylinder of length $L = 25a$. The error bars represent the standard deviation over 40 statistically independent runs. Subfigure (a) The Arc-1-2 polymer is modified to create an additional loop of size 20 within both of its small subloops. Subfigure (b) The Arc-1-2 polymer is modified to create two additional loops, each of size 10, within each of its small subloops. Subfigure (c) The Arc-1-2 polymer is modified to create four additional loops, each of size 5, within each of its small subloops.

Further, we introduce three loops of length 10 monomers into each small subloop of an Arc-1-2 polymer. In Fig.3.14, we plot the positional probability distribution P(z/L)

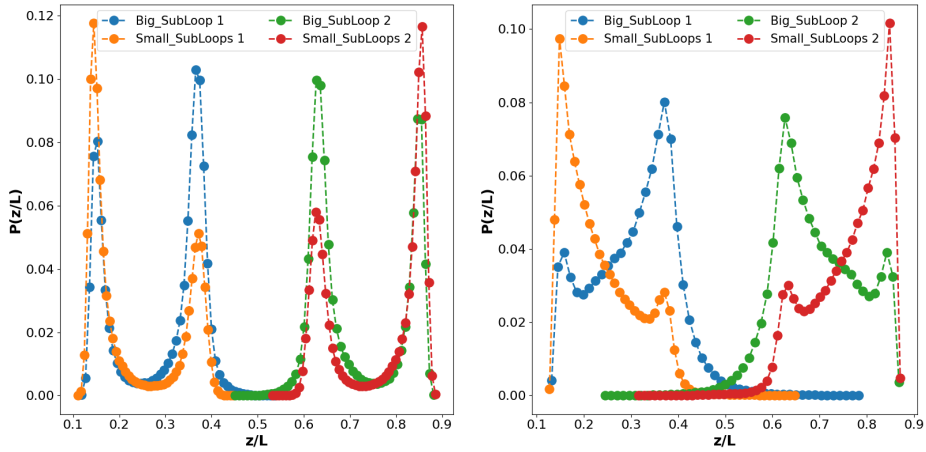

Figure 3.14: Shows the probability distribution P(z/L) of the COM of different subloops with two modified Arc-1-2 polymers. In each small subloop of an Arc-1-2 polymer, we introduce three additional loops of length 10 each. In Subfigure(a), the polymers are confined in a cylinder of length $L = 25a$, while in Subfigure(b), the polymers are confined in a cylinder of length $L = 15a$

of different subloops along the cylinder's axis. We plot the probabilities of the difference configurations (C1, C2, C3 & C4) in Fig.3.15. As shown previously in the case of two Arc-1-2 polymers, we observe a higher inclination for the big subloop to occupy the center of the cylinder as we decrease the cylinder length from $L = 25a$ to $L = 15a$. The increase in the asymmetry of probabilities of C3 & C4 justifies this.

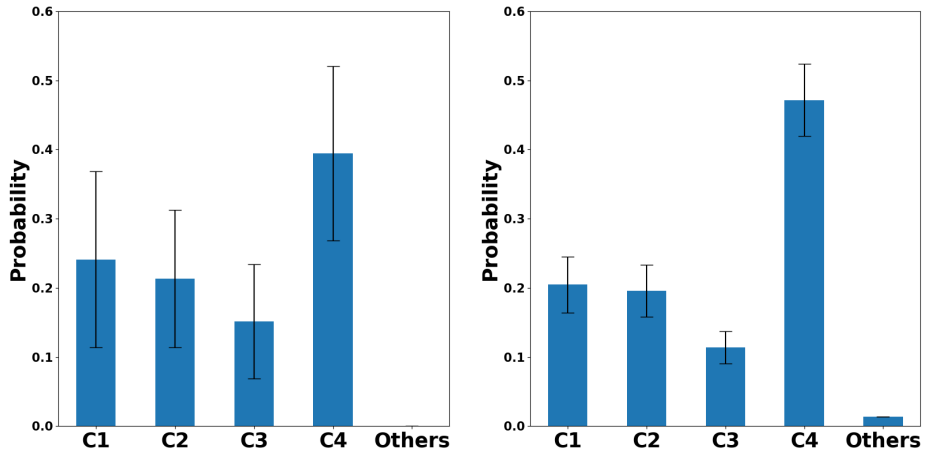

Figure 3.15: Shows the probabilities of the different configurations (C1, C2, C3 & C4) attained by two modified Arc-1-2 polymers. The error bars represent the standard deviation over 40 statistically independent simulations

3.4 The Arc-1-10 Architecture

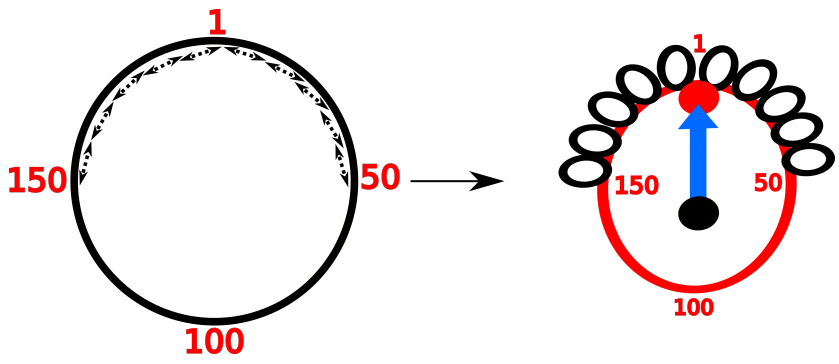

Figure 3.16: Shows a schematic of the Arc-1-10 architecture.

To further enhance this asymmetry, we modify the polymer topology to form multiple small subloops. We create ten CLs in each ring polymer, leading to the formation of one big subloop of 100 monomers and ten smaller subloops of size 10 each. To create this topology, we introduce a cross-link between the monomers (1&10, 11&20, 21&30, 31&40, 41&50, and 151&160, 161&170, 171&180, 181&190, 191&200). We call this topologically modified polymer Arc-1-10. A schematic is provided in Fig.3.16. The probability distribution P(z/L) of the COM positions is plotted in Fig.3.17. Here, we again find four peaks, but there is a stark contrast between the probability distributions of the big and small subloops. We observe a strong inclination for the big subloops to occupy the center. This consequently forces the set of small loops towards the ends of the cylinder. It is important to note that we encounter a few snapshots where the polymers have interchanged positions along the long axis. The existence of a finite probability of the subloops of the first polymer in the right half of the cylinder (and vice versa) justifies this. Interestingly, even in such cases, we observe that the big subloops tend to remain at the center.

To substantiate this, we classify each snapshot and plot probabilities of different configurations C1, C2, C3, and C4 in Fig.3.18. We now see a clear preference for the C4 configuration, with the C4 configuration being about five times more probable than C3 and more than twice as probable than C1 and C2. Through this, we establish that a pair of Arc-1-10 polymers in a cylinder organize themselves such that the big subloops overlap and are present at the center while the set of small loops occupies the ends of the cylinder. We then plot the distribution of $cos(\theta)$ in Fig.3.19, which now again shows an asymmetry in the

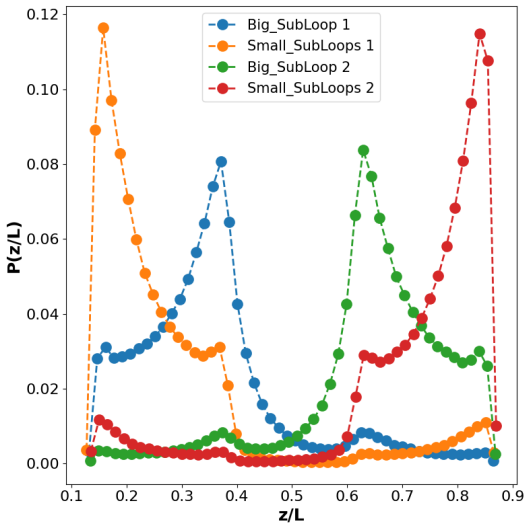

Figure 3.17: Shows the probability distribution P(z/L) of the center of mass (COM) of the different loops as two Arc-1-10 polymers in a cylinder of length $L = 15a$ explore different microstates.

probabilities, with $cos(\theta) = -1$ being three times more probable than $cos(\theta) = 1$. This shows that a higher affinity exists for anti-parallel configurations with two Arc-1-10 polymers.

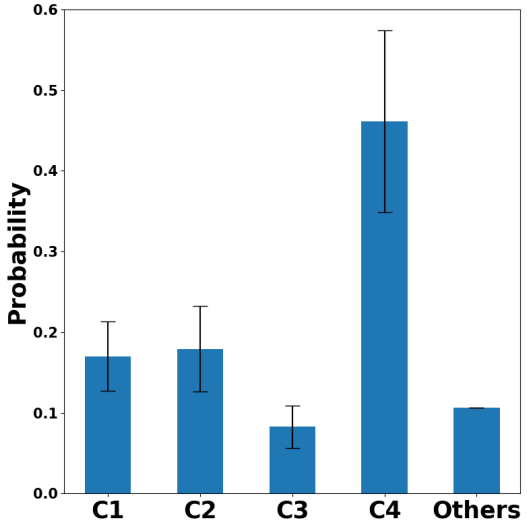

Figure 3.18: Shows the probabilities for different configurations (C1, C2, C3 & C4) with two Arc-1-10 polymers in a cylinder of length $L = 15a$. The error bars represent the standard deviation over 40 statistically independent simulations

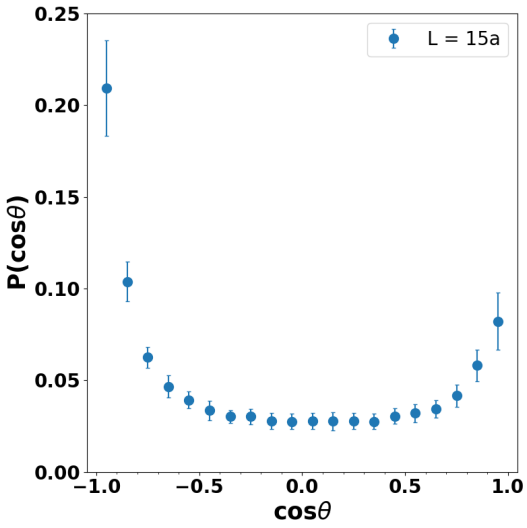

Figure 3.19: Shows the probability distribution of $cos\theta$ for two Arc-1-10 polymers in cylinders of length L = $15a$.

3.5 Radial Organization of two Arc-1-10 Polymers

Here, we look to investigate the radial organization with two Arc-1-10 polymers. We calculate the radial distance from the cylinder axis of each monomer on our system. We plot the monomer distributions of the different subloops separately and find peaks in the distribution, refer to Fig.3.20. We discover that the peaks occur at distances that are a multiple of $0.8a$, i.e., at $0.8a, 1.6a, 2.4a$. We note that $\sigma = 0.8a$ in our simulations. The increasing heights of the peaks result from the greater available volume as we move away from the cylinder axis. On closer inspection, we also find a difference in distributions between the subloops. We observe that at small distances, i.e., close to the cylindrical axis, the probability of finding a monomer belonging to the small subloops is higher. However, moving further along the radius, we are more likely to encounter monomers in the big subloop. This is a consequence of the cross-links(CLs) that form the set of small loops. The set of ten CLs creates a cluster of subloops that localize close to the cylindrical axis. The big subloop is free from this constraint and spreads to occupy larger conformational space around the cylinder.

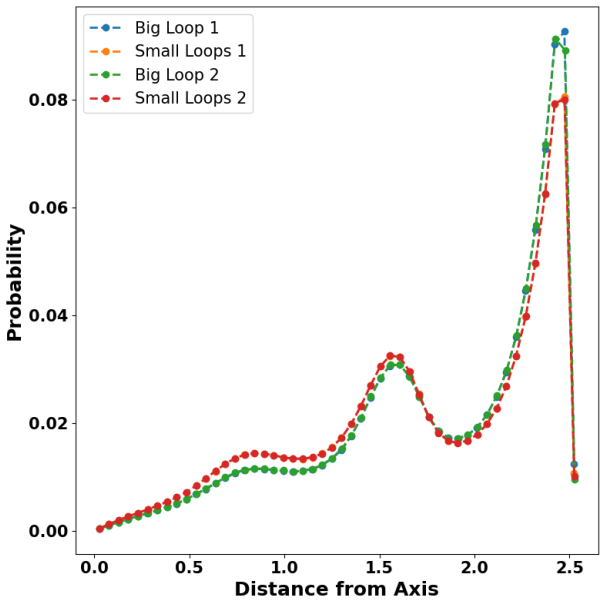

Figure 3.20: This figure shows the monomer density distribution of different subloops for two Arc-1-10 polymers in cylinders of length L = 15a. The distribution for Big Loop 1 and Small Loops 1 exactly overlaps with the corresponding subloops of the second polymer. This is the reason for their lack of visibility in the plot.

3.6 Periodic Boundary Conditions

We now show that this phenomenon is a consequence of the entropic repulsion between the subloops of the polymer and not a boundary effect. To show this, we consider an open cylinder with periodic boundary conditions along the z-axis. It is worth noting that the four distinct configurations in Fig.3.8 now reduce to just two. We can see that configurations C1 & C2 are equivalent, and configurations C3 & C4 are equivalent in the case of periodic boundary conditions along the cylinder axis. We now combine the C1 & C2 configurations and call them 'parallel' and call the C3 & C4 configurations 'Anti-parallel.' In Fig.3.21, we plot the probabilities of these configurations. Again, we see that there is a higher affinity for anti-parallel configurations, i.e., the two polymers self-assemble so that their big loops are in close proximity. Due to periodic boundary conditions, this also means that the smaller subloops lie close to one another. We have previously shown that the overlap of the smaller subloops is highly unfavorable, as evidenced by the low probability of configuration C3 in

Fig.3.4b. Despite this, we find that the smaller subloops approach one another to facilitate the overlap of the big subloops. To substantiate this, we plot the probability distribution of $cos(\theta)$ in Fig.3.22. Again, we see a clear preference for the anti-parallel configuration.

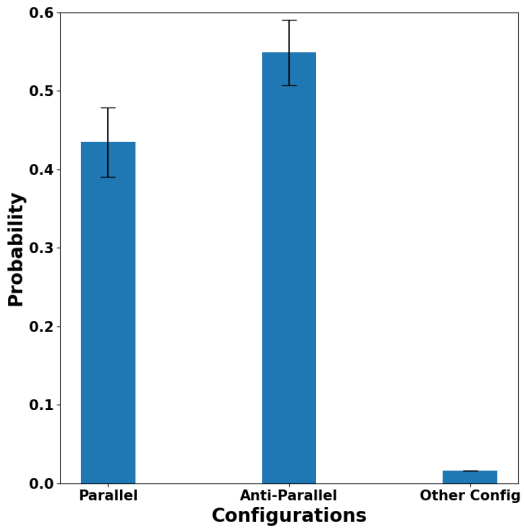

Figure 3.21: Shows the probabilities for Parallel and Anti-parallel configurations with two Arc-1-10 polymers in an open cylinder of length $L = 15a$ and periodic boundary conditions along the cylinder axis.

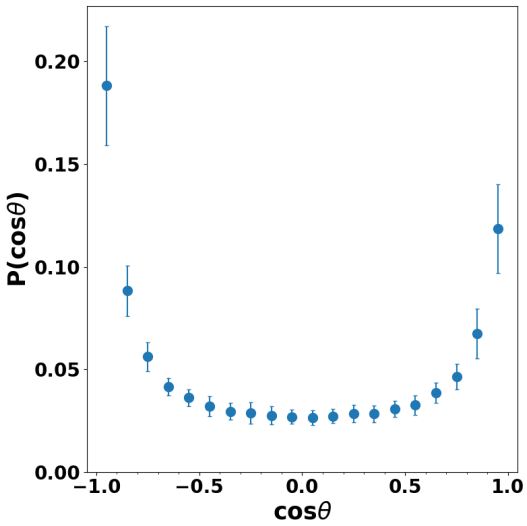

Figure 3.22: Shows the probability distribution of $cos\theta$ for two Arc-1-10 polymers in cylinders of length L = $15a$ and periodic boundary conditions along the cylinder axis.

3.7 Organization in Multiple Polymers

After observing the affinity for anti-parallel configurations with two Arc-1-10 polymers, we investigate if we can observe orientational preference in a system of N polymers within a long cylinder. We begin with three Arc-1-10 polymers in a closed cylinder of length $L = 22.5a$. This maintains the same cylinder length per polymer and, consequently, the same volume fraction. We measure the COM of the different subloops of each polymer and plot the probability distribution along the z-axis in Fig.3.23. We observe six peaks corresponding to the six subloops of the three polymers, indicating that the polymers are well segregated and occupy three separate sections of the cylinder. For the first polymer, we see a higher probability for the set of smaller subloops to occupy the end of the cylinder while the big subloop is present toward the center. Similarly, the third polymer is assembled so that its smaller subloops occupy the cylinder end while the big subloop remains towards the center. We also find that the peaks for the first and third polymers are higher when compared to the polymer in the middle. These polymers have lower motility compared to the central polymer due to the presence of a wall at one of the sides and a polymer on another. However, the central polymer overlaps with the other polymers on both sides, leading to a wider distribution of the COM of its subloops.

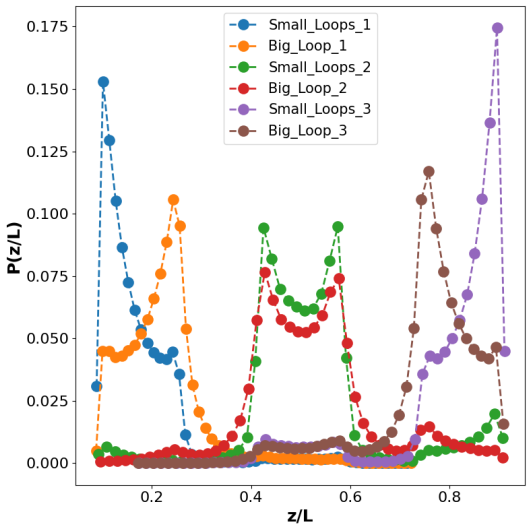

Figure 3.23: Shows probability distribution p(z) of the center of mass (COM) of the different loops as three Arc-1-10 polymers in a cylinder of length $L = 22.5a$ explore different microstates.

As the central polymer overlaps with the big subloops on both sides, the big subloop has an equal probability of overlapping with the big subloop of the first and the third polymer. To substantiate this, we plot the probabilities of all eight configurations in Fig.5.2. We see that the probabilities of configurations 'SB-BS-BS' and 'SB-SB-BS' are equal and are much higher than the rest. This is because both cases involve one overlap of big subloops and one overlap between big and small subloops. We note that every other configuration involves unfavorable overlaps and hence has a lower probability. Similarly, all other equivalent configurations having roughly equal probability show that the data has been averaged over a long time scale such that the system has undergone many flips between the configurations.

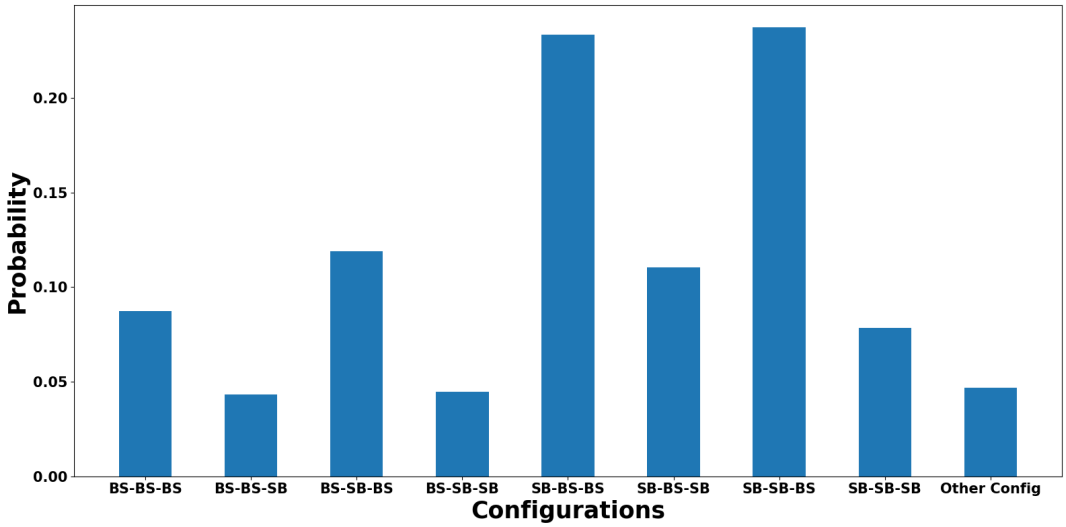

Figure 3.24: Shows the probabilities for different configurations as with three Arc-1-10 polymers in a cylinder of length $L = 22.5a$. With each polymer having two possible orientations, a system of three polymers has eight configurations. Each polymer is classified in an orientation BS, where the vector points to the right, or SB, where the vector points to the left.

We implement the same methodology and confine four such polymers in a cylinder of length $L = 30a$. The spatial probability distribution of the COM of the subloops is plotted in Fig.5.1. Upon careful analysis of the relative probabilities of the subloops, we find that the polymers self-assemble such that the big subloops overlap, followed by the overlap of small subloops. The most probable configuration is depicted in Fig.3.26. In Fig.3.27, we plot the relative probabilities of all vectors being parallel or anti-parallel. The sum of these probabilities is ≈ 0.25. All the other cases are not plotted here as there are 16 different

configurations possible with four such polymers. We conclude that the system is five times more likely to be in an anti-parallel state.

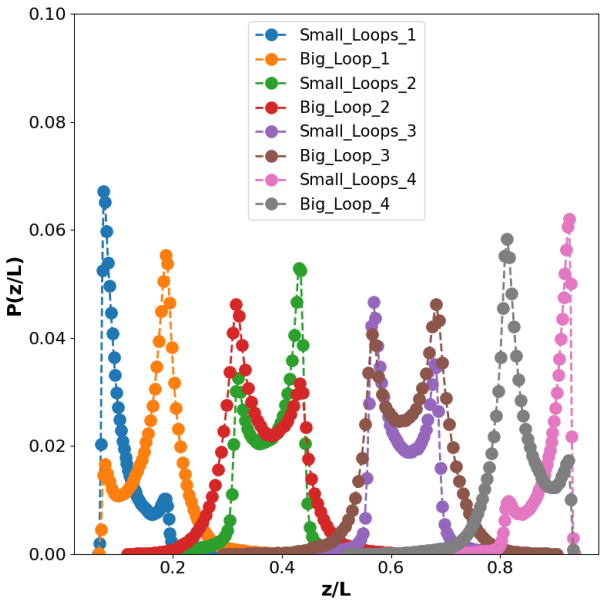

Figure 3.25: Shows the probability distribution P(z/L) of the center of mass (COM) of the different loops as four Arc-1-10 polymers in a cylinder of length $L = 30a$ explore different microstates.

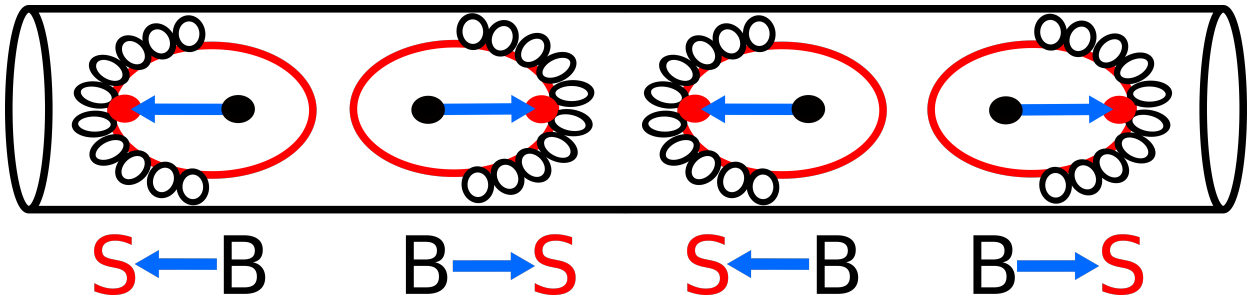

Figure 3.26: Shows a schematic of the most probable configuration attained with four Arc-1-10 polymers in a cylinder of length $L = 30a$. The polymers self-assemble so that vectors of neighboring polymers orient in opposite directions.

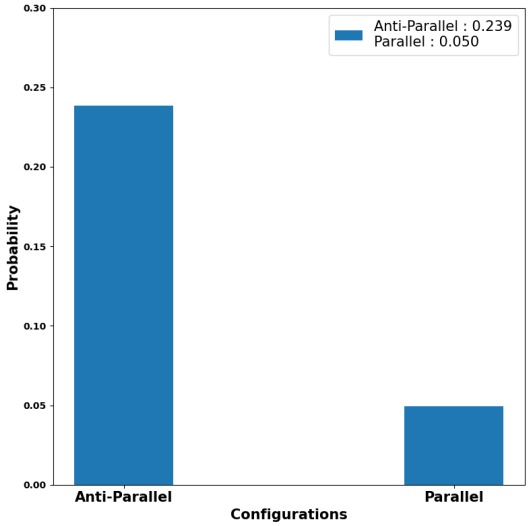

Figure 3.27: Shows the probabilities of all vectors being parallel or anti-parallel to each other in a system of four Arc-1-10 polymers. The system is five times more likely to be in a state where all the vectors are anti-parallel.

To extend this, we consider six and eight Arc-1-10 polymers confined in cylinders of appropriate length. We plot the probability distribution of the subloops in Fig.3.28 Fig.3.29 respectively.

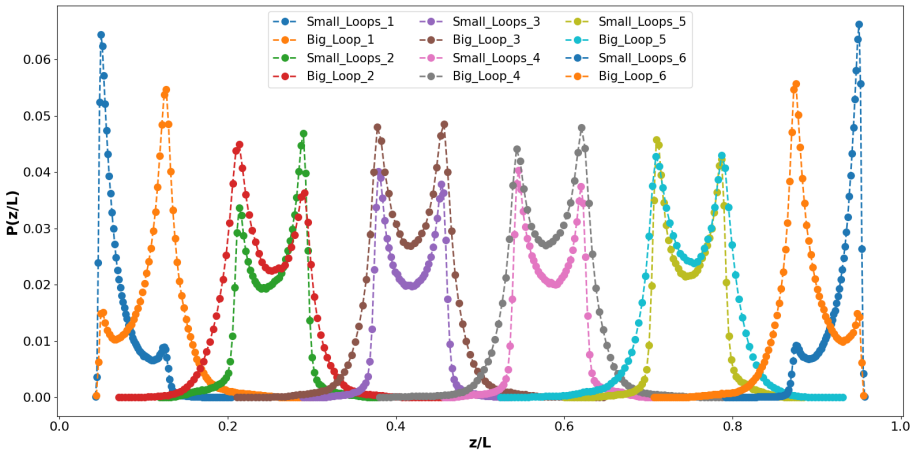

Figure 3.28: Shows the probability distribution P(z/L) of the center of mass (COM) of the different loops as six Arc-1-10 polymers in a cylinder of length $L = 63a$ explore different microstates.

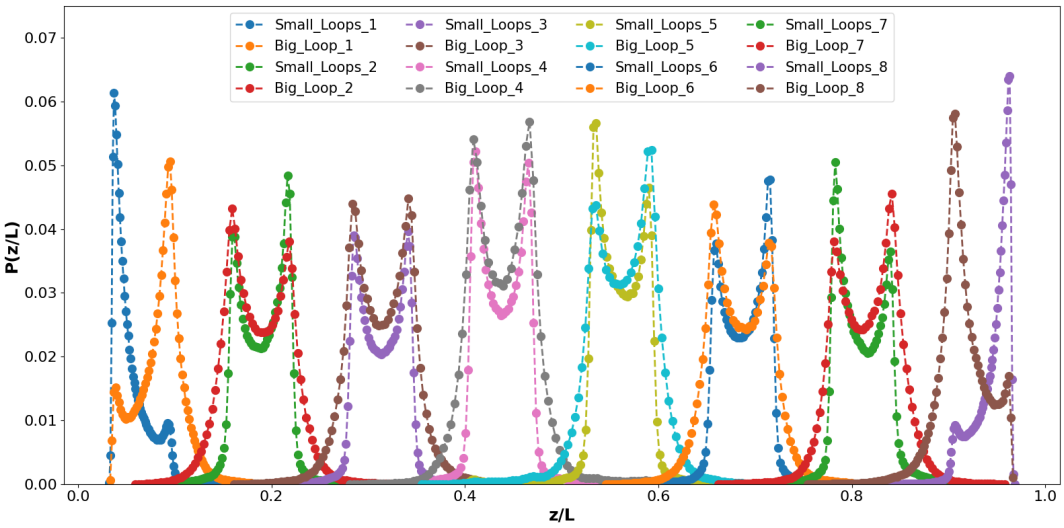

Figure 3.29: Shows the probability distribution P(z/L) of the center of mass (COM) of the different loops as eight Arc-1-10 polymers in a cylinder of length $L = 84a$ explore different microstates.

3.8 Understanding the Hi-C Map

To develop a better understanding of the internal organization of the set of small loops with two Arc-1-10 polymers confined in an open cylinder, we plot a heat map of the contact matrix, refer to Fig.3.30. The matrix element M_{ij} represents the probability of contact between monomers i & j.

To calculate the contact matrix in Fig.3.30, we construct a N $\times$ N matrix where N is the number of particles in the system. Next, we calculate the distance between each pair of particles at each simulation snapshot. Let r_{ij} be the distance between the i^{th} & j^{th} monomers. We consider there is a contact if $r_{ij} \leq 2a$. We append the matrix element M_{ij} by 1. The matrix is constructed by summing over all the snapshots. We normalize the matrix by dividing each element M_{ij} by the sum of the elements in row i. Finally, we plot this matrix as a color map.

The range 1 to 200 corresponds to the monomers of the first polymer, while the monomers 201 to 400 correspond to the monomers of the second polymer. The monomers $51 - -100 -$

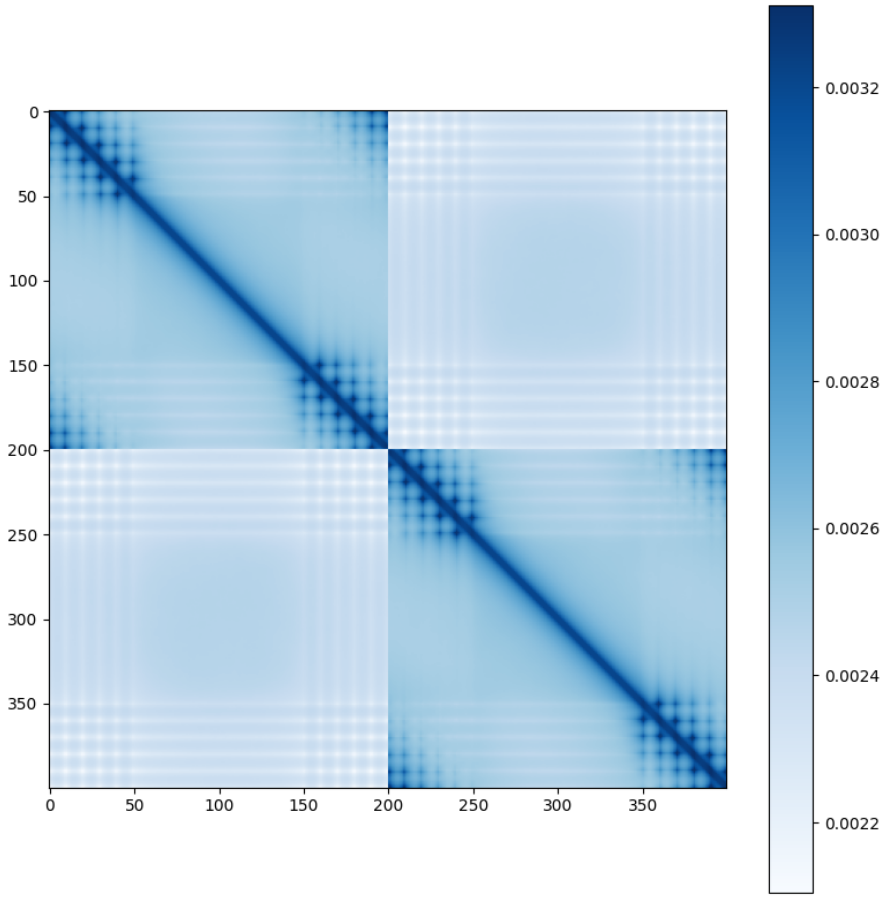

Figure 3.30: Shows the Contact Map with two Arc-1-10 polymers in an open cylinder of length L = 15a. The monomers 1-200 are part of the first polymer, while the monomers 201-400 are part of the second polymer.

-150 ($251--300--350$) are part of the big subloop, while the others are part of the small subloop set. We set the diagonal and next-diagonal elements to zero, as these terms tend to be large and can mask the contributions from the terms away from the diagonal. The figure consists of two dark and two light-colored blocks. The dark block depicts the contact between monomers of the same polymer (intra-polymer), while the lighter block depicts the inter-polymer monomer contacts. The existence of these distinct blocks clearly shows that the polymers are well segregated.

First, we look at the intra-polymer monomer contacts, i.e., the dark blocks. We observe that the dark blocks have a central dark square and a grid-like pattern at their corners. The central dark square signifies the presence of a big subloop, while the grid-like pattern

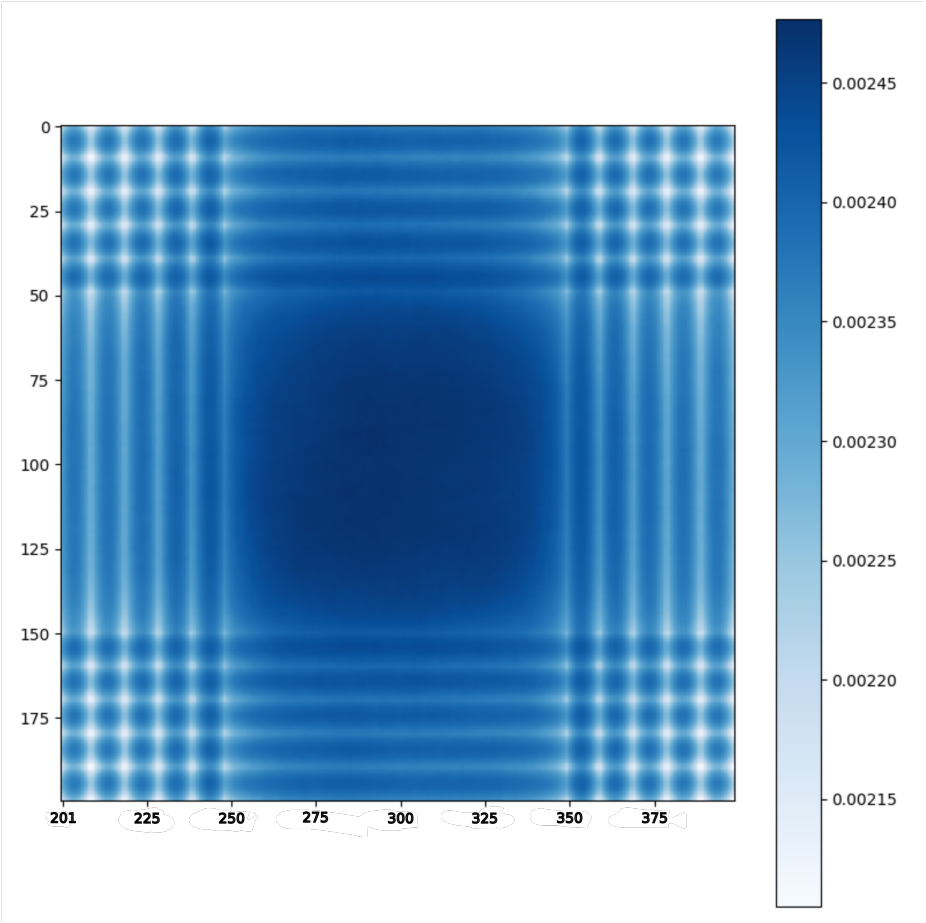

Figure 3.31: Shows a quadrant of the previous Contact Map in greater detail. Here, we plot the contacts between monomers of different polymers.

emerges due to the presence of a continuous set of small loops. The set of continuous CLs brings monomers that are ten units away along the contour close to one another, leading to a grid-like pattern. The lighter areas on all four sides of the central dark square (these areas represent the contacts between the big subloop and the small loops within the same polymer) indicate that the big subloop and the set of small loops avoid each other and remain segregated. We also recognize the presence of alternate dark and light bands in these areas. to understand this, let us consider one small subloop, the loop that is formed by cross-linking monomers 1 and 10. This CL brings these monomers together, creating a 10-monomer loop, where the monomer farthest from the cross-link, that is, 5, is present at the 'tip' of the loop. The presence of a dark line followed by a light band reveals that as one travels from the cross-linked monomer to the tip of the loop, the probability of contact with the big subloop decreases.

Next, we look at the inter-polymer contact between the monomers. To observe the light block closely, we show a zoomed-in picture of the light block in Fig.3.31. We notice a central dark square, which corresponds to the contact probability between monomers $51 - -150$ and $251 - -350$, i;e, the monomers of the big subloops. This is consistent with our previous observation, where we show that the big subloops occupy the center of the cylinder and therefore have a higher frequency of contact. On closer inspection, we also find a grid-like pattern in the four corners of the light block. These represent the contacts between the set of small subloops of the two polymers. The grid-like formation reveals that the inner monomers of the loops are shielded, and the contact between the small subloops happens primarily at the 'tips' of the loops.

Chapter 4

Discussion

In this study, we establish that we indeed observe a preference for certain configurations in the system of flexible polymers. We achieve this by appropriately modifying the topology of a ring polymer. We introduce certain cross-links that create an asymmetry in the structure of a ring polymer. This topological modification, combined with confinement in the cylindrical geometry, induces entropic interactions between segments of neighboring polymers. These induced interactions drive the polymers to self-assemble into structures with higher conformational entropy.

First, we study the organization with two topologically modified ring polymers confined in a cylinder. We create a cross-link (CL) to form two equal-sized subloops. We observe that the polymers remain segregated, and the subloops occupy different segments of the cylinder. This is a consequence of entropic repulsion between different segments of the polymers. When in a mixed state, the polymers have fewer conformational degrees of freedom compared to the case where they are segregated. Based on similar arguments, we show that the internal subloops within the polymer also avoid overlap with one another.

Next, we create an asymmetry in one subloop to create different-sized subloops. We observe the preference for the overlap of the big subloops. Under high confinement, the system chooses to self-assemble whilst facilitating the overlap of the big subloops. The big subloop, which has fewer topological constraints (CLs), can take up a higher number of conformations and is thereby more accommodative to the monomers of the other polymer. However, the set of CLs that form the set of small subloops leads to the clustering of

monomers. This region of high density avoids overlap with other monomers. Therefore, we see a higher preference for the big subloops to occupy the center of the cylinder. This creates a bias for certain orientations in the system of two polymers.

Further, we prove this is not a boundary effect and show that it persists even when considering periodic boundary conditions along the cylinder axis. Next, we show that this phenomenon can be extended to a system of N polymers (though we have considered a maximum of eight polymers in this thesis). We find that the system of N polymers self-assembles such that the big subloops of neighboring polymers overlap. However, this also leads to an overlap of small subloops. Though the overlap of small subloops is entropically unfavorable, the system chooses this configuration. This is because the gain in conformational entropy due to the overlap of big subloops outweighs the loss due to the overlap of small subloops.

Finally, we investigate the organization of subloops in greater detail by plotting a contact map. We gain new insights by thoroughly analyzing the contact map. We confirm our previous finding and observe a greater probability of contact between monomers of the big subloops. The monomers of the small subloops avoid overlap, and their contact primarily happens at the 'tip' of the subloop. The small subloop cluster ensures that the monomers close to the CLs remain shielded from contact.

In the future, one can extend this study by examining the organization and orientation of these topologically modified polymers in a 2-D system. This can studied by confining polymers between horizontal plates (Quasi-2D system).

Though we study the physical aspects of ring polymers with subloops, the architectures we consider in this thesis have biological relevance. In the E.coli DNA, experiments have shown the presence of a certain set of proteins called MukBEF responsible for creating cross-links along the DNA contour[29]. It has been found that MukBEF localizes around the origin of replication (OriC) and forms subloops primarily on one-half of the contour of the DNA. This is similar to the Arc-1-10 architecture we considered. We clarify that, unlike our architectures, the subloops in the DNA are dynamic. The subloops are continuously changing sizes and locations. Despite this, it is worth investigating how these sets of small subloops help the organization and segregation of the E.coli DNA.

Chapter 5

Supplementary Information (SI)

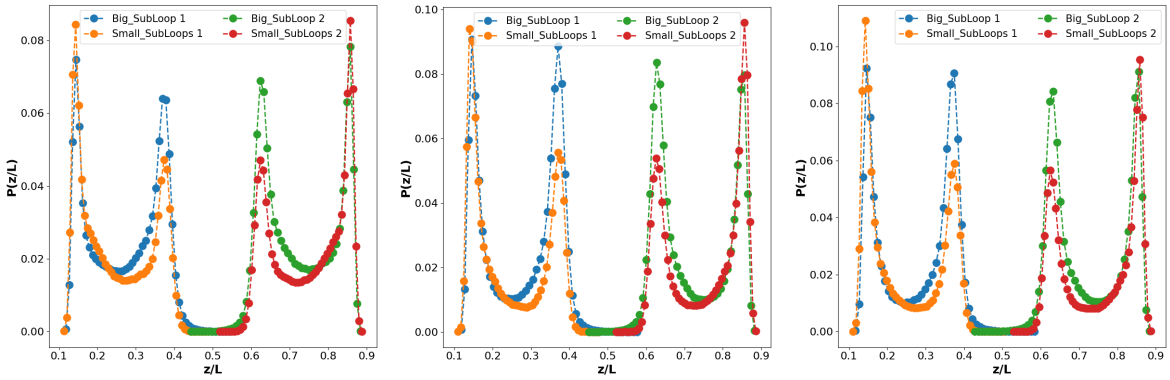

Figure 5.1: Shows the spatial probability distribution P(z/L) of the COM of different subloops along the z-axis with two modified Arc-1-2 polymers in a closed cylinder of length $L = 25a$. Subfigure (a) The Arc-1-2 polymer is modified to create an additional loop of size 20 within both of its small subloops. Subfigure (b) The Arc-1-2 polymer is modified to create two additional loops, each of size 10, within each of its small subloops. Subfigure (c) The Arc-1-2 polymer is modified to create four additional loops, each of size 5, within each of its small subloops.

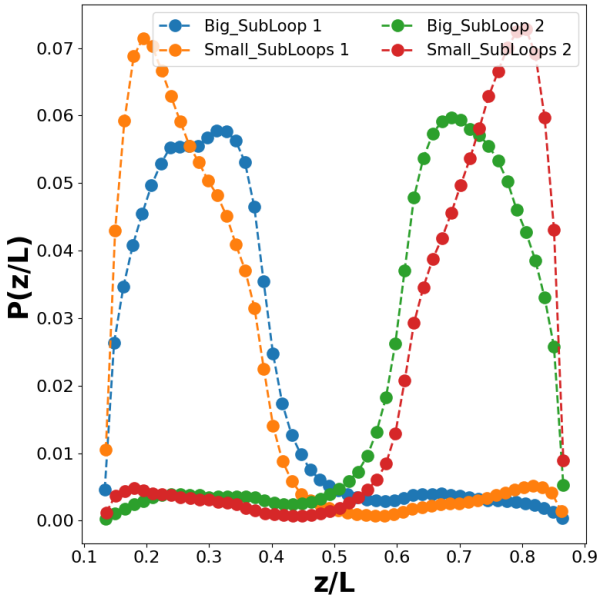

Figure 5.2: Shows the spatial probability distribution P(z/L) of the COM of different subloops along the z-axis. There are two Arc-1-2 polymers with $N = 500$ monomers each confined in a closed cylinder of length $L = 21a$ and diameter $D = 7a$. The dimensions are chosen while maintaining the same aspect ratio and volume fraction considered in the case of $N = 200$ monomers.

Bibliography

[1] Michael Rubinstein and Ralph H Colby. *Polymer Physics*. Oxford University Press, 2003.

[2] A.R. Khokhlov. *Statistical Physics of Macromolecules*. AIP series in polymers and complex materials. AIP Press, 1994.

[3] A.Y. Grosberg and A.R. Khokhlov. *Giant Molecules: Here, There, And Everywhere (2nd Edition)*. World Scientific Publishing Company, 2010.

[4] P. de Gennes. *Scaling concepts in polymer physics*. Cornell Univ. Pr., Ithaca [u.a.], 1979.

[5] Le Guillou, J.C. and Zinn-Justin, J. Accurate critical exponents from field theory. *J. Phys. France*, 50(12):1365–1370, 1989.

[6] Jr. Rouse, Prince E. A Theory of the Linear Viscoelastic Properties of Dilute Solutions of Coiling Polymers. *The Journal of Chemical Physics*, 21(7):1272–1280, 07 1953.

[7] Bruno H. Zimm. Dynamics of Polymer Molecules in Dilute Solution: Viscoelasticity, Flow Birefringence and Dielectric Loss. *The Journal of Chemical Physics*, 24(2):269–278, 02 1956.

[8] Tom McLeish. Polymers without beginning or end. *Science*, 297(5589):2005–2006, September 2002.

[9] Jonathan D Halverson, Jan Smrek, Kurt Kremer, and Alexander Y Grosberg. From a melt of rings to chromosome territories: the role of topological constraints in genome folding. *Reports on Progress in Physics*, 77(2):022601, January 2014.

[10] Christopher W. Bielawski, Diego Benitez, and Robert H. Grubbs. An "endless" route to cyclic polymers. *Science*, 297(5589):2041–2044, September 2002.

[11] Alexander Yu Grosberg, Pavel G Khalatur, and Alexei R Khokhlov. Polymeric coils with excluded volume in dilute solution: The invalidity of the model of impenetrable

spheres and the influence of excluded volume on the rates of diffusion-controlled intermacromolecular reactions. *Die Makromolekulare Chemie, Rapid Communications*, 3(10):709–713, 1982.

[12] AA Louis, PG Bolhuis, JP Hansen, and EJ Meijer. Can polymer coils be modeled as "soft colloids"? *Physical review letters*, 85(12):2522, 2000.

[13] James Dautenhahn and Carol K Hall. Monte carlo simulation of off-lattice polymer chains: effective pair potentials in dilute solution. *Macromolecules*, 27(19):5399–5412, 1994.

[14] S. Jun and B. Mulder. Entropy-driven spatial organization of highly confined polymers: Lessons for the bacterial chromosome. *Proceedings of the National Academy of Sciences*, 103(33):12388–12393, August 2006.

[15] Youngkyun Jung and Bae-Yeun Ha. Overlapping two self-avoiding polymers in a closed cylindrical pore: Implications for chromosome segregation in a bacterial cell. *Phys. Rev. E*, 82(5), November 2010.

[16] Youngkyun Jung, Juin Kim, Suckjoon Jun, and Bae-Yeun Ha. Intrachain ordering and segregation of polymers under confinement. *Macromolecules*, 45(7):3256–3262, March 2012.

[17] Bae-Yeun Ha and Youngkyun Jung. Polymers under confinement: single polymers, how they interact, and as model chromosomes. *Soft Matter*, 11(12):2333–2352, 2015.

[18] Suckjoon Jun, Axel Arnold, and Bae-Yeun Ha. Confined space and effective interactions of multiple self-avoiding chains. *Physical Review Letters*, 98(12), March 2007.

[19] Suckjoon Jun and Andrew Wright. Entropy as the driver of chromosome segregation. *Nature Reviews Microbiology*, 8(8):600–607, August 2010.

[20] J. Pelletier, K. Halvorsen, B.-Y. Ha, R. Paparcone, S. J. Sandler, C. L. Woldringh, W. P. Wong, and S. Jun. Physical manipulation of the escherichia coli chromosome reveals its soft nature. *Proceedings of the National Academy of Sciences*, 109(40):E2649–E2656, September 2012.

[21] Virginia S. Lioy, Axel Cournac, Martial Marbouty, Stéphane Duigou, Julien Mozziconacci, Olivier Espéli, Frédéric Boccard, and Romain Koszul. Multiscale structuring of the e. coli chromosome by nucleoid-associated and condensin proteins. *Cell*, 172(4):771–783.e18, 2018.

[22] Shreerang Pande, Apratim Chatterji, and Debarshi Mitra. Polymer architecture orchestrates the segregation and spatial organization of replicating E.coli chromosomes in slow growth. *Soft Matter*, 2022.

[23] Debarshi Mitra, Shreerang Pande, and Apratim Chatterji. Topology-driven spatial organization of ring polymers under confinement. *Phys. Rev. E*, 106:054502, Nov 2022.

[24] Shreerang Pande, Debarshi Mitra, and Apratim Chatterji. Entropy mediated organization of e.coli chromosome in fast growth conditions, 2023.

[25] John D. Weeks, David Chandler, and Hans C. Andersen. Role of Repulsive Forces in Determining the Equilibrium Structure of Simple Liquids. *The Journal of Chemical Physics*, 54(12):5237–5247, 06 1971.

[26] Don S. Lemons and Anthony Gythiel. Paul Langevin's 1908 paper "On the Theory of Brownian Motion" ["Sur la théorie du mouvement brownien," C. R. Acad. Sci. (Paris) 146, 530–533 (1908)]. *American Journal of Physics*, 65(11):1079–1081, 11 1997.

[27] A. P. Thompson, H. M. Aktulga, R. Berger, D. S. Bolintineanu, W. M. Brown, P. S. Crozier, P. J. in 't Veld, A. Kohlmeyer, S. G. Moore, T. D. Nguyen, R. Shan, M. J. Stevens, J. Tranchida, C. Trott, and S. J. Plimpton. LAMMPS - a flexible simulation tool for particle-based materials modeling at the atomic, meso, and continuum scales. *Comp. Phys. Comm.*, 271:108171, 2022.

[28] Alexander Stukowski. Visualization and analysis of atomistic simulation data with OVITO-the Open Visualization Tool. *MODELLING AND SIMULATION IN MATERIALS SCIENCE AND ENGINEERING*, 18(1), JAN 2010.

[29] Jarno Mäkelä and David J. Sherratt. Organization of the escherichia coli chromosome by a mukbef axial core. *Molecular Cell*, 78(2):250–260.e5, 2020.